

Published in final edited form as:

*Environ Sci Technol.* 2012 January 17; 46(2): 1055–1062. doi:10.1021/es203612d.

## Inhibitory Effect of Dissolved Silica on the H<sub>2</sub>O<sub>2</sub> Decomposition by Iron(III) and Manganese(IV) Oxides: Implications for H<sub>2</sub>O<sub>2</sub>-based In Situ Chemical Oxidation

Anh Le-Tuan Pham<sup>1</sup>, Fiona M. Doyle<sup>2,\*</sup>, and David L. Sedlak<sup>1,\*</sup>

<sup>1</sup>Department of Civil and Environmental Engineering University of California at Berkeley Berkeley, California 94720

<sup>2</sup>Department of Materials Science and Engineering University of California at Berkeley Berkeley, California 94720

### Abstract

The decomposition of H<sub>2</sub>O<sub>2</sub> on iron minerals can generate •OH, a strong oxidant that can transform a wide range of contaminants. This reaction is critical to *In Situ* Chemical Oxidation (ISCO) processes used for soil and groundwater remediation, as well as advanced oxidation processes employed in waste treatment systems. The presence of dissolved silica at concentrations comparable to those encountered in natural waters decreases the reactivity of iron minerals toward H<sub>2</sub>O<sub>2</sub>, because silica adsorbs onto the surface of iron minerals and alters catalytic sites. At circumneutral pH values, goethite, amorphous iron oxide, hematite, iron-coated sand and montmorillonite that were pre-equilibrated with 0.05 – 1.5 mM SiO<sub>2</sub> were significantly less reactive toward H<sub>2</sub>O<sub>2</sub> decomposition than their original counterparts, with the H<sub>2</sub>O<sub>2</sub> loss rates inversely proportional to the SiO<sub>2</sub> concentration. In the goethite/H<sub>2</sub>O<sub>2</sub> system, the overall •OH yield, defined as the percentage of decomposed H<sub>2</sub>O<sub>2</sub> producing •OH, was almost halved in the presence of 1.5 mM SiO<sub>2</sub>. Dissolved SiO<sub>2</sub> also slows the H<sub>2</sub>O<sub>2</sub> decomposition on manganese(IV) oxide. The presence of dissolved SiO<sub>2</sub> results in greater persistence of H<sub>2</sub>O<sub>2</sub> in groundwater, lower H<sub>2</sub>O<sub>2</sub> utilization efficiency and should be considered in the design of H<sub>2</sub>O<sub>2</sub>-based treatment systems.

### Introduction

The injection of oxidants into the subsurface is a widely used approach for remediating soils and groundwater contaminated with organic compounds. This method, known as *In Situ* Chemical Oxidation (ISCO), is attractive because it requires less infrastructure investment and has lower maintenance and operation cost than pump-and-treat remediation.<sup>1</sup> Furthermore, the relatively fast production of oxidants expedites completion of site remediation.

Among various oxidants employed in ISCO (i.e., permanganate, hydrogen peroxide, ozone and persulfate)<sup>1</sup>, hydrogen peroxide (H<sub>2</sub>O<sub>2</sub>) is probably the most widely used, because it is relatively inexpensive, easy to transport and introduce into the subsurface, and the byproducts of H<sub>2</sub>O<sub>2</sub> decomposition, namely O<sub>2</sub> and H<sub>2</sub>O, are benign. H<sub>2</sub>O<sub>2</sub>-based ISCO

\*Address correspondence to either author. fmdoyle@berkeley.edu (F.M.D.). \*sedlak@berkeley.edu (D.L.S.). Phone: +1-510-642-5771 (F.M.D.); +1-510-643-0256 (D.L.S.).

**Supporting Information** Figure S1–S7, Column experiments with β-MnO<sub>2</sub> and FeOOH, role of H<sub>2</sub>O<sub>2</sub> diffusion and H<sub>2</sub>O<sub>2</sub> adsorption on the rate of H<sub>2</sub>O<sub>2</sub> decomposition by goethite. This information is available free of charge via the Internet at <http://pubs.acs.org/>

technologies rely on the conversion of  $\text{H}_2\text{O}_2$  into hydroxyl radical ( $\bullet\text{OH}$ ), either by reactions with subsurface materials (e.g., iron-containing clays and minerals) or by reactions with dissolved ferrous ions that are sometimes co-injected with  $\text{H}_2\text{O}_2$ .<sup>1,2</sup> However, the rapid loss of  $\text{H}_2\text{O}_2$  upon injection is often problematic because  $\text{H}_2\text{O}_2$  may decompose before it reaches contaminated zones.<sup>1,3</sup> Consequently, a large excess of  $\text{H}_2\text{O}_2$  is often used and injection wells have to be constructed immediately proximate to contaminated areas.

The rate at which  $\text{H}_2\text{O}_2$  decomposes and the fraction of the  $\text{H}_2\text{O}_2$  converted into  $\bullet\text{OH}$  depends upon the composition of the aquifer materials and groundwater. Iron oxides (e.g., ferrihydrite or goethite) convert  $\text{H}_2\text{O}_2$  into  $\bullet\text{OH}$  through a surface-initiated chain reaction analogous to the Haber-Weiss mechanism.<sup>2,4–6</sup> Iron oxides also can convert  $\text{H}_2\text{O}_2$  directly into  $\text{O}_2$  and  $\text{H}_2\text{O}$  via two-electron transfer mechanisms.<sup>5,6</sup> In contrast, manganese oxides do not generate  $\bullet\text{OH}$  when they decompose  $\text{H}_2\text{O}_2$ .<sup>5,7</sup> In the subsurface,  $\text{H}_2\text{O}_2$  can also be decomposed by (e.g., catalases and peroxidases) via pathways that also do not produce  $\bullet\text{OH}$ .<sup>5</sup> Conversely, the presence of phosphate<sup>8</sup> or metal complexing ligands, such as citrate and phytate<sup>9</sup>, enhance the stability of  $\text{H}_2\text{O}_2$  because they can bind metals and decrease their reactivity. The efficacy of  $\text{H}_2\text{O}_2$ -based ISCO, therefore, depends on the  $\text{H}_2\text{O}_2$  persistence as well as the pathways through which it is decomposed, because only those that produce  $\bullet\text{OH}$  will be beneficial for oxidative contaminant removal. A thorough understanding of how different subsurface components affect the decomposition of  $\text{H}_2\text{O}_2$  will, therefore, help to predict its fate and could lead to an ability to improve the performance of  $\text{H}_2\text{O}_2$ -based ISCO.

The aim of this research was to investigate the effect of dissolved  $\text{SiO}_2$  on the rate of  $\text{H}_2\text{O}_2$  decomposition catalyzed by different types of iron- and manganese- containing materials. Silica is particularly important to ISCO, because depending on local geology, groundwater can contain dissolved  $\text{SiO}_2$  at concentration ranging from 5 mg/L to 85 mg/L (i.e., 0.08 – 1.42mM  $\text{SiO}_2$ ).<sup>10</sup> Although dissolved  $\text{SiO}_2$  adsorbs on the surface of iron oxides<sup>11,12</sup> and  $\text{SiO}_2$  is known to act as corrosion inhibitor, its effect on  $\text{H}_2\text{O}_2$  decomposition in the subsurface, to the best of our knowledge, has not been investigated previously. Therefore, the rate of  $\text{H}_2\text{O}_2$  decomposition on goethite, hematite, amorphous iron oxyhydroxide, iron-coated sand, montmorillonite and pyrolusite was studied in solutions containing various amount of dissolved  $\text{SiO}_2$  (i.e., 0 – 1.5 mM  $\text{SiO}_2$ ). To gain insight into the impact of  $\text{SiO}_2$  on the performance of ISCO, the effect of dissolved  $\text{SiO}_2$  on the overall  $\bullet\text{OH}$  yield, defined as the percentage of decomposed  $\text{H}_2\text{O}_2$  producing  $\bullet\text{OH}$ , was also investigated.

## Materials and Methods

### Chemicals

Amorphous iron oxyhydroxide (i.e.,  $\text{FeOOH}$ ) was obtained from Aldrich, while pyrolusite ( $\beta\text{-MnO}_2$ ) was obtained from Fisher. Wyoming montmorillonite (Swy-2, 31.8  $\text{m}^2/\text{g}$ , 2.59 wt % Fe) was obtained from the Source Clays Repository (The Clay Minerals Society). All other chemicals were reagent grade from Fisher Scientific and were used without further purification.

Goethite and hematite were synthesized following procedures reported in the literature<sup>13</sup> and their identity was verified by X-ray diffraction. Briefly, goethite was synthesized by aging freshly made ferrihydrite in a strong alkaline solution ( $\text{NaOH}$ ) at 70°C for 60 hours. Hematite was synthesized using the same method except that the aging was conducted at pH 8 – 8.5 in the presence of  $\text{NaHCO}_3$  at 90°C for 48 hrs. Amorphous  $\text{FeOOH}$  50 – 80 mesh was ground using a mortar and pestle prior to sieving through a 150 micron sieve.

The surface area of these solids, determined using the 5 point BET (Brunauer–Emmett–Teller) nitrogen physisorption method, was 21.8  $\text{m}^2/\text{g}$  for hematite, 19  $\text{m}^2/\text{g}$  for goethite,

165.8 m<sup>2</sup>/g for FeOOH, and less than 1 m<sup>2</sup>/g for MnO<sub>2</sub>. Iron-coated sand (1 wt% Fe, 4.8 m<sup>2</sup>/g) was kindly provided by Peter Nico (Lawrence Berkeley National Laboratory). The synthesis and characterization of iron-coated sand have been reported elsewhere.<sup>14</sup>

A stock solution of 15 mM silica was prepared daily from Na<sub>2</sub>SiO<sub>3</sub>·9H<sub>2</sub>O. For simplicity, all species of dissolved silica (e.g., H<sub>4</sub>SiO<sub>4</sub>, H<sub>3</sub>SiO<sub>4</sub><sup>−</sup> and polymeric silica) are denoted as SiO<sub>2</sub>. All solutions were prepared using 18 MΩ Milli-Q water from a Millipore system.

## Experimental setup

All experiments were carried out at 25 ± 1 °C in the dark in a 50-mL polypropylene flask open to the atmosphere. The temperature was controlled with a water bath. The pH of solutions was buffered with 1 mM piperazine-N,N'-bis(ethanesulfonic acid) (PIPES) for pH 7 or 4 mM borate for pH 8 – 9. The ionic strength of the solutions was maintained with 0.1 M NaNO<sub>3</sub>. The pH was measured throughout each experiment and was adjusted when it deviated from the initial value by more than 0.1 unit. Experiments were conducted at least in triplicate and average values along with one standard deviation are presented.

**Adsorption of dissolved SiO<sub>2</sub> by the solids**—Silica was added from a 15 mM stock solution to the buffered solutions and the pH was adjusted with 1 M NaOH or 0.5 M H<sub>2</sub>SO<sub>4</sub>. To minimize the polymerization and avoid SiO<sub>2(s)</sub> precipitation, SiO<sub>2</sub> concentrations never exceeded 1.5 mM.<sup>15</sup> Next, a solid (i.e., iron oxide, iron coated sand, Swy-2 or pyrolusite) was added to the solution and the pH again was adjusted if necessary. Samples were withdrawn at pre-determined time intervals. Within 5 minutes, the solid was separated by centrifugation, then the supernatant was filtered immediately through a 0.2-μm nylon filter and analyzed for dissolved SiO<sub>2</sub>.

**H<sub>2</sub>O<sub>2</sub> decomposition and phenol oxidation**—The decomposition of H<sub>2</sub>O<sub>2</sub> catalyzed by the solids was investigated in the absence and presence of dissolved SiO<sub>2</sub>. Prior to the addition of H<sub>2</sub>O<sub>2</sub>, suspensions were mixed for 24 hrs to equilibrate the solids with SiO<sub>2</sub>. All experiments with iron-containing minerals were performed in pH 7 ± 0.1 solutions. Experiments with β-MnO<sub>2</sub> were conducted at pH 8.4 because the 1 mM PIPES buffer was ineffective at pH 7.0. At pH 8.4, the pH never changed by more than 0.1 units during the experiments.

To investigate the effect of dissolved SiO<sub>2</sub> on •OH production, the transformation of 0.2 mM phenol in the goethite/H<sub>2</sub>O<sub>2</sub> system was studied. Phenol was chosen as a model target contaminant because it is not significantly adsorbed by any of the solids and reacts with •OH at a near-diffusion controlled rate. Samples were withdrawn at predetermined time intervals and divided into two parts. In the first aliquot, the solids were separated by centrifugation followed by filtration and the solution was analyzed for H<sub>2</sub>O<sub>2</sub>. Acetonitrile was added to the second aliquot (acetonitrile:sample = 1:1) and the mixture was agitated vigorously for 2 minutes with a vortex mixer to extract any adsorbed phenol from the solids. The solids were then separated by centrifugation and filtration and the solution was analyzed for phenol. Phenol recovery by acetonitrile extraction was always above 98% in H<sub>2</sub>O<sub>2</sub>-free controls. The stoichiometric efficiency, defined as the amount of phenol transformed per mole of

hydrogen peroxide decomposed (i.e.,  $E = \frac{\Delta[\text{phenol}]}{\Delta[\text{H}_2\text{O}_2]} \times 100\%$ ),<sup>6</sup> was used to evaluate the effect of dissolved SiO<sub>2</sub> on •OH production.

## Analytical methods

Phenol was analyzed using HPLC as described previously.<sup>6</sup> H<sub>2</sub>O<sub>2</sub> was analyzed spectrophotometrically by the titanium sulfate method.<sup>16</sup> An inductively coupled plasma

optical emission spectrometer (ICP-OES) was used to measure dissolved  $\text{SiO}_2$ ; all results are reported in molar based on the  $\text{SiO}_2$  formula. Total dissolved iron was quantified using the 1,10-phenanthroline method<sup>17</sup> after adding hydroxylamine hydrochloride to the filtered samples. The concentration of dissolved iron was always below the detection limit (i.e., 5  $\mu\text{M}$ ).

Goethite surfaces, pre-equilibrated with  $\text{SiO}_2$  solutions, were examined with a Philips CM200/FEG transmission electron microscope coupled with an energy dispersive X-ray unit (EDX). The instrument was operated in scanning mode (STEM/EDX) with a probe size 1.4 nm. Samples for STEM/EDX analysis were prepared as follows: after the adsorption experiment, the solid was collected by centrifugation and then resuspended in 2 mL fresh Milli-Q water. An aliquot of this suspension was spread on the copper grid, the excess water was gently removed with a Kimwipe tissue and the grid was dried under air at room temperature.

## Results

### Silica adsorption

The rate of silica adsorption onto goethite, hematite and Swy-2 in pH 7 solutions with different  $[\text{SiO}_2]_{\text{initial}}$  was investigated. In all cases,  $\text{SiO}_2$  adsorption approached equilibrium within 24 hrs (inset of Figure 1 and Figure S1 in Supporting Information). Therefore,  $\text{SiO}_2$  adsorption as a function of  $[\text{SiO}_2]_{\text{initial}}$  was measured after a 24 hr equilibration period. This equilibration period was also employed in the study of  $\text{H}_2\text{O}_2$  decomposition and phenol transformation.

Higher initial  $\text{SiO}_2$  concentrations resulted in more  $\text{SiO}_2$  adsorption onto goethite (Figure 1). Except for the last data point in Figure 1 ( $[\text{SiO}_2]_{\text{equilibrium}} = 1.14 \text{ mM}$ ), the adsorption isotherm followed a Langmuir-type isotherm, with a maximum adsorption density ( $\Gamma_{\text{SiO}_2}$ ) of approximately 0.062 mmol  $\text{SiO}_2/\text{g}$  goethite (Figure 1). At  $[\text{SiO}_2]_{\text{equilibrium}} = 1.14 \text{ mM}$ , the amount  $\text{SiO}_2$  sorbed was significantly higher (0.09 mmol  $\text{SiO}_2/\text{g}$  goethite).

STEM/EDX analysis indicated that  $\text{SiO}_2$  was not uniformly adsorbed on the goethite surface. For example, EDX spectra of a goethite sample that was pre-equilibrated with 0.5 mM  $\text{SiO}_2$  for 24 hrs showed that the surface elemental composition varied among locations (Figure 2), with Si peaks not observed in some locations (Figure 2a), co-occurring with iron in others (Figure 2b) and existing in the absence of an iron peak in others (Figure 2c). The fraction of sites that were fully coated with Si (i.e., sites having EDX spectra similar to that of Figure 2c) increased as the  $[\text{SiO}_2]_{\text{initial}}$  increased.

### $\text{H}_2\text{O}_2$ decomposition and phenol transformation

In the  $\text{SiO}_2$ -free system, the half-life of 5 mM  $\text{H}_2\text{O}_2$  in the presence of 4 g/L goethite was  $7.77 \pm 0.34 \text{ hr}$  (Table 1). Addition of dissolved  $\text{SiO}_2$  slowed the rate of  $\text{H}_2\text{O}_2$  decomposition, increasing the  $\text{H}_2\text{O}_2$  half-life to  $21.7 \pm 1.2$  and  $28.2 \pm 1.8$  at an  $[\text{SiO}_2]_{\text{initial}}$  of 0.5 mM and 1.5 mM, respectively (Table 1 and Figure 3a). The half-life of  $\text{H}_2\text{O}_2$  in the presence of  $[\text{SiO}_2]_{\text{initial}} = 1.5 \text{ mM}$  was comparable to that observed in a solution containing 2 mM phosphate ( $t_{1/2} = 31.6 \pm 1.4$ , Table 1). Under the experimental conditions employed in this study, the  $\text{H}_2\text{O}_2$  decomposition rate was limited by the intrinsic chemical reactivity of the solids and not by diffusion of  $\text{H}_2\text{O}_2$  to the surface or the number of sites available for  $\text{H}_2\text{O}_2$  adsorption (see Supporting Information for detailed discussion). The observed-first order rate constant of  $\text{H}_2\text{O}_2$  decomposition ( $k_{\text{obs}}$ ) was inversely proportional to the amount of  $\text{SiO}_2$  in the solution (Figure 3b). At adsorption densities below 0.04 mmol/g goethite,  $k_{\text{obs}}$  decreased linearly with the  $\text{SiO}_2$  adsorption density, with a slope of  $-0.303 \text{ hr}^{-1} \cdot \text{mmol}^{-1} \cdot \text{gram}$ . At adsorption densities above 0.04 mmol/g goethite,  $k_{\text{obs}}$  was much less

sensitive to increasing adsorption density (the slope of the regression line was  $-0.036 \text{ hr}^{-1} \cdot \text{mmol}^{-1} \cdot \text{gram}$ ). The presence of dissolved  $\text{SiO}_2$  also diminished the rate of  $\text{H}_2\text{O}_2$  loss catalyzed by other iron-containing minerals (Table 1). In the presence of 0.5 mM  $[\text{SiO}_2]_{\text{initial}}$ , the half-life of  $\text{H}_2\text{O}_2$  increased by at least a factor of two compared with the  $\text{SiO}_2$ -free system in all cases.

To understand the effect of dissolved  $\text{SiO}_2$  on the efficiency of the conversion of  $\text{H}_2\text{O}_2$  into  $\bullet\text{OH}$  by iron-containing minerals, the oxidation of phenol in the goethite/ $\text{H}_2\text{O}_2$  system was investigated. Typical phenol transformation data are presented in Figure 4a, which shows that silica slowed the rate of both  $\text{H}_2\text{O}_2$  decomposition and phenol transformation. A control experiment indicated no phenol loss in the absence of  $\text{H}_2\text{O}_2$ . Addition of 100 mM tert-butanol, a  $\bullet\text{OH}$  scavenger, completely eliminated phenol degradation (data not shown), confirming that the loss of phenol observed was due to reaction with  $\bullet\text{OH}$ . In the absence of dissolved  $\text{SiO}_2$ , the stoichiometric efficiency throughout the course of the experiment ranged from 0.25 to 0.3%. The stoichiometric efficiency was slightly lower in the presence of  $[\text{SiO}_2]_{\text{initial}} = 0.5 \text{ mM}$ , while at  $[\text{SiO}_2]_{\text{initial}} = 1.5 \text{ mM}$  the efficiency ranged from 0.14 to 0.2% (Figure 4b).

### Pyrolusite

The adsorption of dissolved silica onto  $\beta\text{-MnO}_2$  and its effect on the catalytic activity of  $\beta\text{-MnO}_2$  toward  $\text{H}_2\text{O}_2$  decomposition were also investigated (Figure 5). In the  $\text{SiO}_2$ -free system, 50 mM  $\text{H}_2\text{O}_2$  was decomposed within 2 hours. As with iron-containing materials, addition of dissolved  $\text{SiO}_2$  slowed the rate of  $\text{H}_2\text{O}_2$  decomposition in proportion to the concentration of added  $\text{SiO}_2$ . The half-life of  $\text{H}_2\text{O}_2$  was approximately 0.15 hr for the  $\text{SiO}_2$ -free system and 0.5 hr for the experiment with 1.5 mM  $\text{SiO}_2$ . Unlike the case with iron oxides, the adsorption of  $\text{SiO}_2$  was not measurable even at a  $\beta\text{-MnO}_2$  concentration of 20 g/L (inset of Figure 5).

### Discussion

Adsorption of  $\text{SiO}_2$  affects the surface properties and reactivity of metal oxides and clays in natural and engineered processes. For example, the presence of dissolved  $\text{SiO}_2$  inhibits the nucleation and growth of iron precipitates<sup>18</sup> as well as the transformation of amorphous iron (hydr)oxide into more stable phases (e.g., goethite).<sup>19</sup> Dissolved  $\text{SiO}_2$  also appears to stabilize iron oxide colloids, enhancing their mobility in natural waters and decreasing the efficiency of iron-based coagulation processes employed in drinking and wastewater treatment operation.<sup>20–22</sup> Adsorption of  $\text{SiO}_2$  also alters the surface area, charge and surface complexation sites on iron oxides, thereby affecting the adsorption of various solutes.<sup>19,23–25</sup> The presence of  $\text{SiO}_2$  in water also affects the corrosion of iron, with sorbed  $\text{SiO}_2$  forming a protective layer that inhibits corrosion<sup>26,27</sup> or an impurity that destabilizes protective iron oxide scale layers.<sup>27</sup>

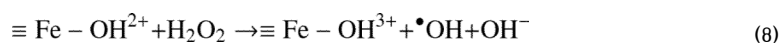
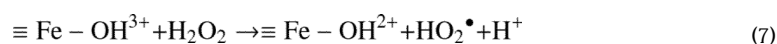
In our experimental system, silica slowed the rate of  $\text{H}_2\text{O}_2$  decomposition on iron and manganese mineral surfaces (Figure 3 and 5). To understand how  $\text{SiO}_2$  affects the reactivity of minerals in this process, it is necessary to understand how  $\text{SiO}_2$  and  $\text{H}_2\text{O}_2$  interact with metal-containing surfaces. The adsorption behavior of  $\text{SiO}_2$  on iron minerals is presented below, followed by a discussion of  $\text{H}_2\text{O}_2$  decomposition mechanisms and the possible effects of  $\text{SiO}_2$ . As the mechanism through which  $\text{H}_2\text{O}_2$  is decomposed on  $\text{MnO}_2$  differs from that of iron minerals, the  $\text{MnO}_2$  system is discussed separately.

## Iron minerals

SiO<sub>2</sub> adsorption often exhibits a fast and a slow stage, with more than 90% of adsorption taking place within the first few hours and the remaining 10% of adsorption occurring over several weeks (Figure 1 and S1).<sup>12,28</sup> Solution conditions such as pH and SiO<sub>2</sub>-to-iron oxide ratio strongly affect this process.<sup>12,28</sup> In addition to the bulk solution measurements, spectroscopic techniques such as ATR-IR<sup>29</sup> and XAFS<sup>18</sup>, as well as surface modeling tools, have been used to infer the bonding of sorbed SiO<sub>2</sub> and the mechanism through which adsorption occurs. The adsorption process generally has been described as a complexation reaction between surface hydroxyl groups and SiO<sub>2</sub>. However, no consensus has been reached on the exact nature of this interaction at a molecular level. Some investigators argued that the process involves the reaction between a monomeric SiO<sub>2</sub> species and one hydroxyl group (reaction (1) and (2) in Table 2).<sup>11,30</sup> However, Davis *et al.* invoked SiO<sub>2</sub> adsorption by both monomeric and dimeric species (reaction (3) and (4)) to explain adsorption data along with the zeta potential data.<sup>12</sup> It also has been suggested that adsorption can involve a bidentate complex between an SiO<sub>2</sub> monomer and 2 hydroxyl groups (reaction (5))<sup>18,28</sup> and that the siloxane linkages could form between two adjacent sorbed SiO<sub>2</sub> monomers or/and between sorbed monomers and dissolved SiO<sub>2</sub> (reaction (6)).<sup>29,31</sup> The latter scenario might lead to the formation of oligomeric silica species (e.g., a linear trimer<sup>29</sup>, or cyclic tetramer<sup>32</sup>) on the surface. The difference in the behavior of surface-adsorbed SiO<sub>2</sub> could be attributable to differences in solution conditions that were employed in these studies. Polymeric silica species tend to be important at high pH and high SiO<sub>2</sub> concentrations<sup>12</sup> while a high SiO<sub>2</sub>-to-iron oxide ratio could result in a high density of sorbed SiO<sub>2</sub> ( $\Gamma_{Si}$ ), leading to the formation of oligomeric species.

In the present study, we used STEM/EDX to investigate the distribution of Si on the surface of goethite that had been pre-equilibrated with solutions containing varying amounts of dissolved SiO<sub>2</sub>. With a nano-sized probe (1.4 nm in this study), STEM/EDX is capable of providing a high resolution elemental distribution map that cannot be obtained by other techniques (e.g., scanning electron microscopy/EDX or X-ray photoelectron spectroscopy). A nano-sized probe technique is also needed to evaluate heterogeneity of the small goethite particles employed in this study (less than 100 nm, Figure S4). The relatively heterogeneous distribution of Si on the goethite surface and the presence of regions that were fully coated with Si (Figure 2) suggest that the adsorption did not take place in a “layer-by-layer” mode, presumably because adsorption is more favorable on some crystallographic faces than on others. The presence of more regions that were fully coated with Si at higher [SiO<sub>2</sub>]<sub>initial</sub> supports the hypothesis that a high SiO<sub>2</sub>-to-iron oxide ratio leads to the formation of oligomeric species.

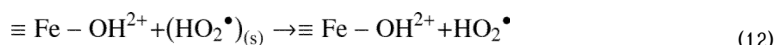
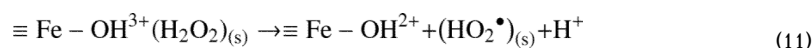
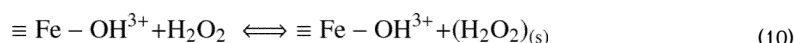
**Hydrogen peroxide decomposition**—Iron oxides and iron-containing (e.g., ferrihydrite, goethite, iron-containing clays and iron-coated sand) can catalyze the decomposition of H<sub>2</sub>O<sub>2</sub>. This process can generate hydroxyl radical (•OH), presumably through a Haber – Weiss mechanism analogous to that observed in the homogeneous Fenton system:<sup>2,4,5,33</sup>







Some investigators have postulated that, as in the homogeneous Fenton system, reaction (7) actually consists of a series of reactions, beginning with the formation of a complex between the surface and  $\text{H}_2\text{O}_2$ :<sup>33,34</sup>



Assuming that reaction (10) is the first step in  $\text{H}_2\text{O}_2$  decomposition, sorbed  $\text{SiO}_2$  may alter the reactivity of iron minerals by occupying iron surface hydroxyl groups, thereby preventing the formation of  $\equiv \text{Fe} - \text{OH}^{3+} (\text{H}_2\text{O}_2)_{(\text{s})}$ . As mentioned above, the  $\text{SiO}_2$  adsorption mechanism is not totally understood. Therefore, we did not try to estimate the number of hydroxyl groups that were occupied by  $\text{SiO}_2$  and consequently, no correlation between the number of available hydroxyl groups with  $k_{\text{obs}}$  has been made. However, the  $\Gamma_{\text{Si}} - k_{\text{obs}}$  profile (Figure 3b) supports the hypothesis that the slower decomposition of  $\text{H}_2\text{O}_2$  was due to occupation of surface sites by  $\text{SiO}_2$ . At a  $\Gamma_{\text{Si}} < 0.04$  mmol/g goethite, where regions that were fully covered with Si were negligible,  $k_{\text{obs}}$  drastically decreased as  $\Gamma_{\text{Si}}$  increased. Due to the formation of oligomeric species at higher  $\Gamma_{\text{Si}}$ , the number of iron sites that were occupied by  $\text{SiO}_2$  only increased slightly, resulting in a much slower  $k_{\text{obs}}$  decrease in this range. The higher  $\Gamma_{\text{Si}}$  observed at  $[\text{SiO}_2]_{\text{equilibrium}} = 1.14$  mM (Figure 1) also could be attributable to the formation of oligomeric species. Finally, the presence of sites that were not occupied with Si (Figure 2a) could help to explain why  $\text{H}_2\text{O}_2$  decomposition in all experiments was still observed at high  $\text{SiO}_2$  concentration.

It was previously observed that under circumneutral pH conditions,  $\text{H}_2\text{O}_2$  decomposes mainly through pathways that do not produce  $\bullet\text{OH}$ .<sup>5,6</sup> Consequently, understanding the branching between different pathways is important because only those that produce  $\bullet\text{OH}$  will be beneficial for contaminant oxidation. Our data (Figure 4) indicate that dissolved  $\text{SiO}_2$  has a detrimental effect on the overall stoichiometric efficiency. A possible explanation might be that surface sites have different reactivity toward  $\bullet\text{OH}$  production and the preferential adsorption of  $\text{SiO}_2$  on “more  $\bullet\text{OH}$  productive” sites would lower the stoichiometric efficiency. Although assigning surface sites with different affinities is used widely in describing adsorption on iron oxides<sup>35</sup>, the above hypothesis is speculative and further research is needed to address this issue.

### Pyrolusite

Manganese oxides (such as birnessite and pyrolusite) are very reactive in catalyzing  $\text{H}_2\text{O}_2$  decomposition. Although the mechanism of this process remains unclear, our data (Figure S5) and those of other investigators<sup>1,5,7</sup> indicate that this process does not produce  $\bullet\text{OH}$ . Consequently, the presence of  $\text{MnO}_2$  in aquifer materials is detrimental for  $\text{H}_2\text{O}_2$ -based ISCO.

H<sub>2</sub>O<sub>2</sub> decomposition by  $\beta$ -MnO<sub>2</sub> also slowed in the presence of dissolved SiO<sub>2</sub>, although the mechanism through which the loss of H<sub>2</sub>O<sub>2</sub> was inhibited is unclear. In a batch experiment with  $\beta$ -MnO<sub>2</sub>, SiO<sub>2</sub> adsorption was not measurable (inset of Figure 5). We were also unable to find any reports of adsorption of SiO<sub>2</sub> onto MnO<sub>2</sub>, suggesting that SiO<sub>2</sub> does not adsorb on MnO<sub>2</sub> to an appreciable extent. However, it would be difficult to measure minor adsorption in the batch tests, even with the highest solids density tested. A column experiment was used to assess the potential for SiO<sub>2</sub> adsorption at higher  $\beta$ -MnO<sub>2</sub> concentrations (refer to the Supporting Information for experimental setup). The results show that there was, indeed, a modest degree of silica uptake onto the  $\beta$ -MnO<sub>2</sub> from the solution during the first few minutes of the test, the uptake being proportional to the amount of MnO<sub>2</sub> in the column (Figure S6). This modest uptake of silica is likely to be responsible for the lower reactivity of MnO<sub>2</sub> observed experimentally. However, further research is needed to address this issue.

### Environmental implications

The results of this study suggest that in H<sub>2</sub>O<sub>2</sub>-based ISCO systems, H<sub>2</sub>O<sub>2</sub> should last longer if groundwater contains a significant amount of dissolved SiO<sub>2</sub>. In systems where the subsurface is deficient in SiO<sub>2</sub>, dissolved silica could be injected together with H<sub>2</sub>O<sub>2</sub> to increase the persistence of H<sub>2</sub>O<sub>2</sub> to assure remediation of areas further from the injection well. Dissolved SiO<sub>2</sub> has a potential to be a better H<sub>2</sub>O<sub>2</sub>-stabilizing agent than phosphate because SiO<sub>2</sub> is inexpensive and does not stimulate bacterial growth. Although SiO<sub>2</sub> decreased the stoichiometric yield of •OH from iron minerals, this effect was relatively modest, and would be outweighed in *in situ* applications by the greater longevity of H<sub>2</sub>O<sub>2</sub> in the presence of SiO<sub>2</sub>. The effect of SiO<sub>2</sub>, however, will vary among aquifers with different mineral compositions (e.g., iron and manganese content and crystallinity, soil organic matter content) and groundwater chemistry. These factors should be considered in the design and operation of H<sub>2</sub>O<sub>2</sub>-based ISCO. Additionally, because silica adsorption is a reversible process (Figure S7), it would appear advisable to inject dissolved SiO<sub>2</sub> and H<sub>2</sub>O<sub>2</sub> simultaneously to assure H<sub>2</sub>O<sub>2</sub> lifetime enhancement.

Our study also indicates that many bench-scale studies performed in the absence of dissolved SiO<sub>2</sub> may have underestimated the lifetime of H<sub>2</sub>O<sub>2</sub> or overestimated the effect of stabilizing agents. For example, in the SiO<sub>2</sub>-free system (H<sub>2</sub>O<sub>2</sub> half-life of 7.77 hr, Table 1), 2 mM phosphate increased the H<sub>2</sub>O<sub>2</sub> half-life by approximately a factor of four ( $t_{1/2}$  = 31.6 hr). In the presence of 0.5 mM SiO<sub>2</sub>, however, phosphate provided much less of an effect, increasing the half-life of H<sub>2</sub>O<sub>2</sub> by about only 50% ( $t_{1/2}$  = 21.7 hr and 33.5 hr in the absence and presence of phosphate, respectively).

SiO<sub>2</sub> also suppressed H<sub>2</sub>O<sub>2</sub> decomposition by MnO<sub>2</sub>. Depending on the relative amount of iron- and manganese-containing solids, SiO<sub>2</sub> could enhance the overall efficiency of the remediation process, especially in soils with high Mn content. Additional research is needed to assess the contribution of different iron- and manganese-containing solids to H<sub>2</sub>O<sub>2</sub> loss in soils and aquifer materials.

Finally, our data also suggest that dissolved silica can affect the reactivity of iron-containing catalysts used in H<sub>2</sub>O<sub>2</sub>-based advanced oxidation processes. Although the SiO<sub>2</sub> concentrations in surface waters and industrial wastes are often lower than those observed in groundwater, a gradual loss in catalyst activity due to SiO<sub>2</sub> adsorption will likely occur during long-term catalyst use.



## Acknowledgments

This research was funded by the U.S. National Institute for Environmental Health Sciences (NIEHS) Superfund Basic Research Program (Grant P42 ES004705). The authors acknowledge support of the National Center for Electron Microscopy, Lawrence Berkeley National Laboratory, which is supported by the U.S. Department of Energy under Contract # DE-AC02-05CH11231. A.L.P. was supported in part by Vietnam Education Foundation (VEF).

## References

1. Huling, SG.; Pivetz, BE. In-Situ Chemical Oxidation. U.S. Environmental Protection Agency Engineering Issue. 2006. [http://www.epa.gov/ada/topics/oxidation\\_pubs.html](http://www.epa.gov/ada/topics/oxidation_pubs.html)
2. Pignatello JJ, Oliveros E, MacKay A. Advanced oxidation processes for organic contaminant destruction based on the Fenton reaction and related chemistry. *Critical Reviews in Environmental Science and Technology*. 2006; 36:1.
3. Watts RJ, Teel AL. Chemistry of modified Fenton's reagent (catalyzed H<sub>2</sub>O<sub>2</sub> propagations-CHP) for in situ soil and groundwater remediation. *Journal of Environmental Engineering-ASCE*. 2005; 131:612–622.
4. Kwan WP, Voelker BM. Decomposition of hydrogen peroxide and organic compounds in the presence of dissolved iron and ferrihydrite. *Environmental Science & Technology*. 2002; 36:1467–1476. [PubMed: 11999052]
5. Petigara BR, Blough NV, Mignerey AC. Mechanisms of hydrogen peroxide decomposition in soils. *Environmental Science & Technology*. 2002; 36:639–645. [PubMed: 11878378]
6. Pham AL-T, Lee C, Doyle FM, Sedlak DL. A silica-supported iron oxide catalyst capable of activating hydrogen peroxide at neutral pH values. *Environmental Science & Technology*. 2009; 43:8930–8935. [PubMed: 19943668]
7. Furman O, Laine DF, Blumenfeld A, Teel AL, Shimizu K, Cheng IF, Watts RJ. Enhanced reactivity of superoxide in water–solid matrices. *Environmental Science & Technology*. 2009; 43:1528–1533. [PubMed: 19350930]
8. Kakarla PKC, Watts RJ. Depth of Fenton-like oxidation in remediation of surface soil. *Journal of Environmental Engineering-ASCE*. 1997; 123:11–17.
9. Watts RJ, Finn DD, Cutler LM, Schmidt JT, Teel AL. Enhanced stability of hydrogen peroxide in the presence of subsurface solids. *Journal of Contaminant Hydrology*. 2007; 91:312–326. [PubMed: 17196706]
10. Langmuir, D. *Aqueous Environmental Geochemistry*. Prentice-Hall, Inc.; 1997.
11. Sigg L, Stumm W. The interaction of anions and weak acids with the hydrous goethite ( $\alpha$ -FeOOH) surface. *Colloids and Surfaces*. 1981; 2:101–117.
12. Davis CC, Chen H-W, Edwards M. Modeling silica sorption to iron hydroxide. *Environmental Science & Technology*. 2002; 36:582–587. [PubMed: 11878370]
13. Schwertmann U, Cornell RM. *Iron Oxides in the Laboratory: Preparation and Characterization*. 2000
14. Nico PS, Stewart BD, Fendorf S. Incorporation of oxidized uranium into Fe (hydr)oxides during Fe(II) catalyzed remineralization. *Environmental Science & Technology*. 2009; 43:7391–7396. [PubMed: 19848151]
15. Kohn T, Kane SR, Fairbrother DH, Roberts AL. Investigation of the inhibitory effect of silica on the degradation of 1,1,1-Trichloroethane by granular iron. *Environmental Science & Technology*. 2003; 37:5806–5812. [PubMed: 14717199]
16. Eisenberg G. *Colorimetric determination of hydrogen peroxide*. Industrial & Engineering Chemistry Analytical Edition. 1943; 15:327.
17. Tamura H, Goto K, Yotsuyanagi T, Nagayama M. Spectrophotometric determination of iron(II) with 1,10-phenanthroline in the presence of large amounts of iron(III). *Talanta*. 1974; 21:314. [PubMed: 18961462]
18. Pokrovski GS, Schott J, Farges F, Hazemann J-L. Iron (III)-silica interactions in aqueous solution: insights from X-ray absorption fine structure spectroscopy. *Geochimica et Cosmochimica Acta*. 2003; 67:3559–3573.

19. Anderson PR, Benjamin MM. Effect of silicon on the crystallization and adsorption properties of ferric oxides. *Environmental Science & Technology*. 1985; 19:1048–1053.
20. Cameron AJ, Liss PS. The stabilization of “dissolved” iron in freshwaters. *Water Research*. 1984; 18:179–185.
21. Browman MG, Robinson RB, Reed GD. Silica polymerization and other factors in iron control by sodium silicate and sodium hypochlorite additions. *Environmental Science & Technology*. 1989; 23:566–572.
22. Robinson RB, Frasier B, Reed GD. Iron and manganese sequestration facilities using sodium-silicate. *Journal American Water Works Association*. 1992; 84:77.
23. Davis CC, Knocke WR, Edwards M. Implications of aqueous silica sorption to iron hydroxide: Mobilization of iron colloids and interference with sorption of arsenate and humic substances. *Environmental Science & Technology*. 2001; 35:3158–3162. [PubMed: 11505993]
24. Zachara JM, Girvin DC, Schmidt RL, Resch CT. Chromate adsorption on amorphous iron oxyhydroxide in the presence of major groundwater ions. *Environmental Science & Technology*. 1987; 21:589–594. [PubMed: 19994980]
25. Jordan N, Lomenech C, Marmier N, Giffaut E, Ehrhardt J-J. Sorption of selenium(IV) onto magnetite in the presence of silicic acid. *Journal of Colloid and Interface Science*. 2009; 329:17–23. [PubMed: 18947836]
26. Sastra, VS. *Corrosion Inhibitors. Principles and Applications*. Wiley; West Sussex, England: 1998.
27. Rushing JC, McNeill LS, Edwards M. Some effects of aqueous silica on the corrosion of iron. *Water Research*. 2003; 37:1080–1090. [PubMed: 12553983]
28. Hiemstra T, Barnett MO, van Riemsdijk WH. Interaction of silicic acid with goethite. *Journal of Colloid and Interface Science*. 2007; 310:8–17. [PubMed: 17306821]
29. Swedlund PJ, Hamid RD, Miskelly GM. Insights into  $\text{H}_4\text{SiO}_4$  surface chemistry on ferrihydrite suspensions from ATR-IR, Diffuse Layer Modeling and the adsorption enhancing effects of carbonate. *Journal of Colloid and Interface Science*. 2010; 352:149–157. [PubMed: 20832078]
30. Jordan N, Marmier N, Lomenech C, Giffaut E, Ehrhardt J-J. Sorption of silicates on goethite, hematite, and magnetite: Experiments and modelling. *Journal of Colloid and Interface Science*. 2007; 312:224–229. [PubMed: 17467724]
31. Swedlund PJ, Webster JG. Adsorption and polymerisation of silicic acid on ferrihydrite, and its effect on arsenic adsorption. *Water Research*. 1999; 33:3413–3422.
32. Icopini GA, Brantley SL, Heaney PJ. Kinetics of silica oligomerization and nanocolloid formation as a function of pH and ionic strength at 25°C. *Geochimica et Cosmochimica Acta*. 2005; 69:293–303.
33. Lin S-S, Gurol MD. Catalytic Decomposition of hydrogen peroxide on iron oxide: Kinetics, Mechanism, and Implications. *Environmental Science & Technology*. 1998; 32:1417–1423.
34. Kwan WP, Voelker BM. Rates of hydroxyl radical generation and organic compound oxidation in mineral-catalyzed Fenton-like systems. *Environmental Science & Technology*. 2003; 37:1150–1158. [PubMed: 12680668]
35. Dzombak, DA.; Morel, FM. *Surface complexation modeling: hydrous ferric oxide*. John Wiley & Sons; New York: 1990.

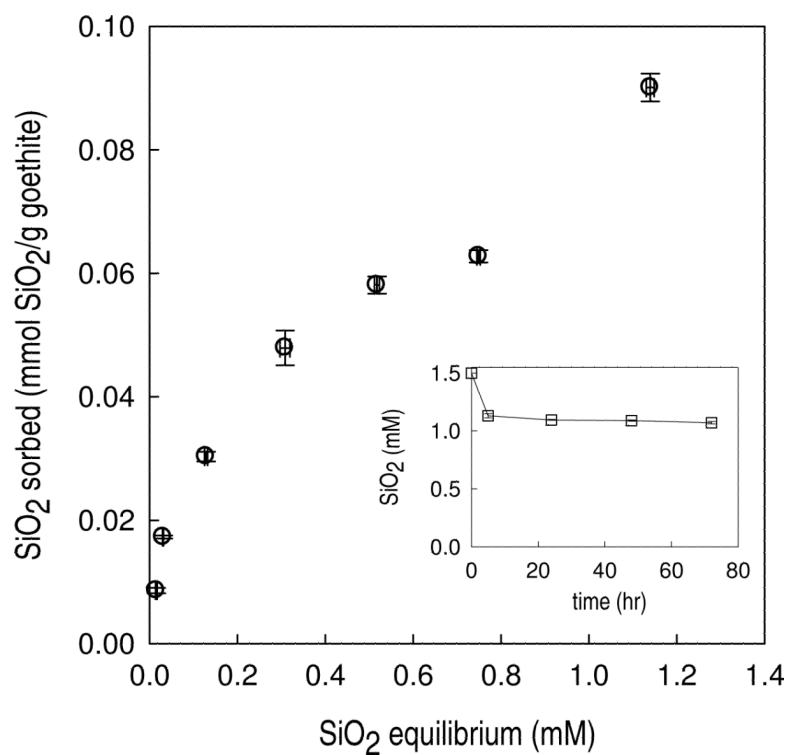


**Figure 1.**

Adsorption isotherm (24 hour equilibration) of dissolved  $\text{SiO}_2$  on goethite. [goethite] = 4 g/L, [PIPES] = 1 mM,  $[\text{NaNO}_3]$  = 0.1 M, pH = 7.  $[\text{SiO}_2]_{\text{initial}}$  = 0 – 1.5 mM (inset: adsorption kinetics).

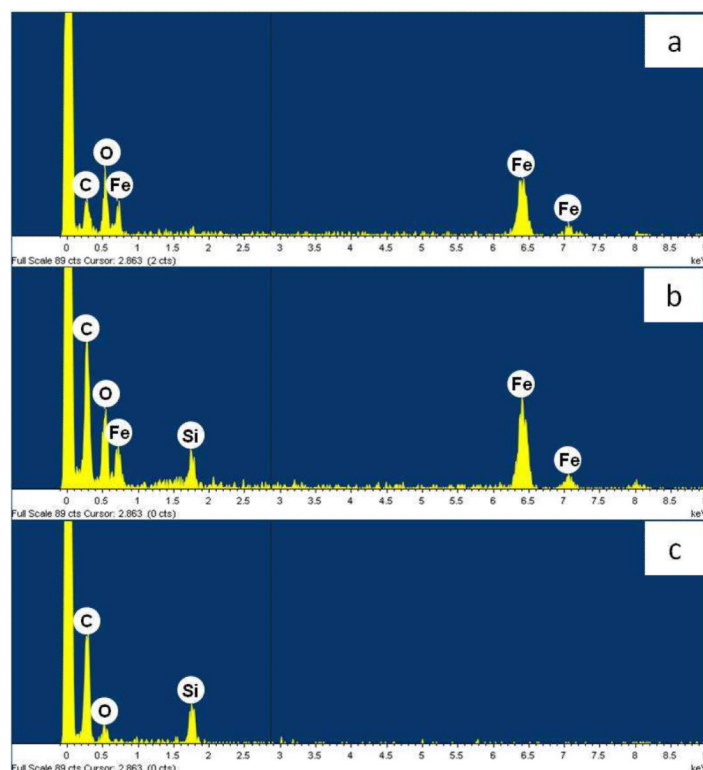


**Figure 2.** EDX spectra from three different locations on a goethite surface that was pre-equilibrated with 0.5 mM dissolved silica solution for 24 hrs. Carbon peaks come from the grid support.

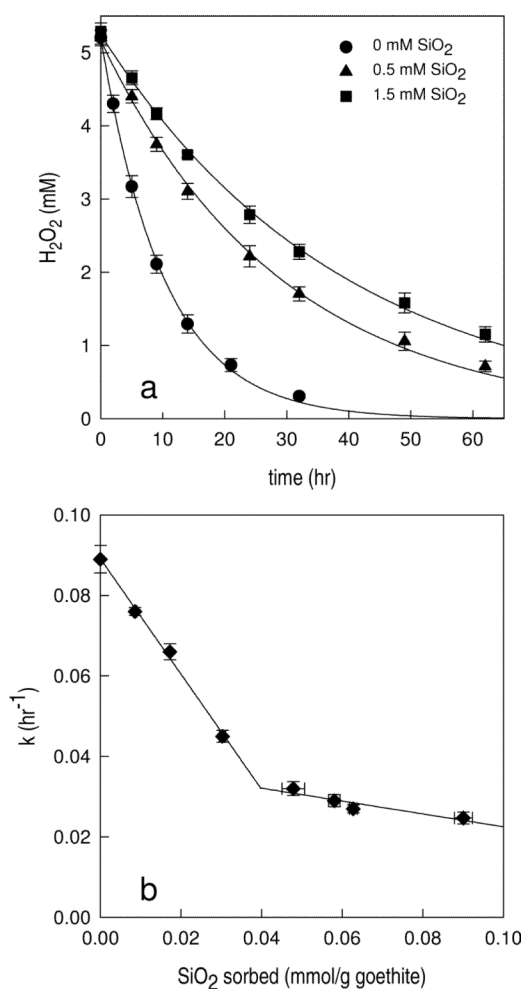


**Figure 3.** Effect of dissolved  $\text{SiO}_2$  on  $\text{H}_2\text{O}_2$  decomposition by goethite.  $[\text{goethite}] = 4 \text{ g/L}$ ,  $[\text{H}_2\text{O}_2]_{\text{initial}} = 5.1 \pm 0.1 \text{ mM}$ ,  $\text{pH} = 6.9 \pm 0.1$ ,  $[\text{PIPES}] = 1 \text{ mM}$ ,  $[\text{NaNO}_3] = 0.1 \text{ M}$ . Solid lines are first-order fit of  $\text{H}_2\text{O}_2$  decomposition (a) and linear fits of first order rate constant  $k_{\text{obs}}$  vs.  $\text{SiO}_2$  sorbed (b).

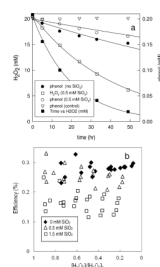


**Figure 4.**

(a):  $H_2O_2$  decomposition (left axis) and phenol transformation (right axis) catalyzed by goethite. Solid line: first order fit to the data. (b): stoichiometric efficiency in the presence of dissolved silica. Experiments were conducted at least triplicate and, instead of present the average value and standard deviation, all results were presented.  $[goethite] = 4 \text{ g/L}$ ,  $pH = 7$ ,  $[PIPES] = 1 \text{ mM}$ ,  $[NaNO_3] = 0.1 \text{ M}$ . Except for the control experiment (inversed triangles), the  $H_2O_2$  initial concentration in all experiments was  $[H_2O_2]_0 = 20 \text{ mM}$ .



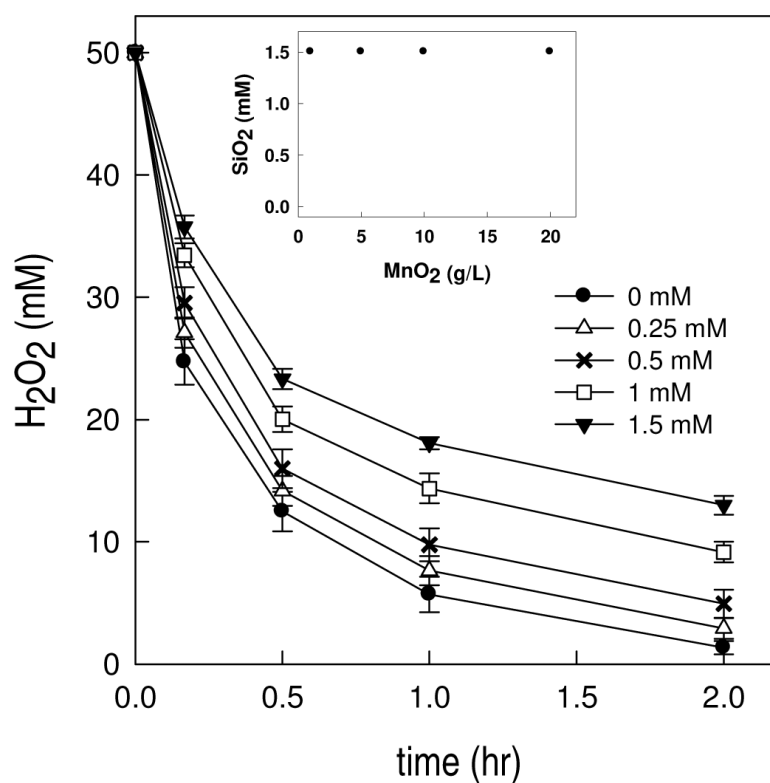


**Figure 5.**

Decomposition of  $\text{H}_2\text{O}_2$  catalyzed by pyrolusite ( $\beta\text{-MnO}_2$ ) in the presence of various concentrations of dissolved  $\text{SiO}_2$ . [ $\beta\text{-MnO}_2$ ] = 1 g/L, pH = 8.4, [ $\text{NaNO}_3$ ] = 0.1 [borate] = 4 mM. Inset: [ $\text{SiO}_2$ ] remaining in the solution after 24 hr equilibration with various amount of  $\text{MnO}_2$ . [ $\text{SiO}_2$ ]<sub>initial</sub> = 1.5 mM, [ $\text{MnO}_2$ ] = 1 – 20 g/L, other conditions were similar to those above.

**Table 1**

Observed-first order rate constants ( $k_{\text{obs}}$ ) for  $\text{H}_2\text{O}_2$  decomposition catalyzed by iron-containing minerals under various conditions.

	Experiment condition	$\text{H}_2\text{O}_2 k_{\text{obs}} (\text{h}^{-1})$	$\text{H}_2\text{O}_2$ half-life (h)
1	4g/L goethite, 0 mM $\text{SiO}_2$	$0.089 \pm 0.003$	$7.77 \pm 0.34$
2	4g/L goethite, 0.5 mM $\text{SiO}_2$	$0.032 \pm 0.002$	$21.7 \pm 1.2$
3	4g/L goethite, 1.5 mM $\text{SiO}_2$	$0.025 \pm 0.002$	$28.2 \pm 1.8$
4	4g/L goethite, 2 mM phosphate	$0.022 \pm 0.001$	$31.6 \pm 1.4$
5	4g/L goethite, 0.5 mM $\text{SiO}_2$ and 2 mM phosphate	$0.021 \pm 0.001$	$33.5 \pm 1.3$
6	4g/L hematite, 0 mM $\text{SiO}_2$	$0.018 \pm 0.002$	$39.4 \pm 3.5$
6	4g/L hematite, 0.5 mM $\text{SiO}_2$	$0.009 \pm 0.001$	$77.7 \pm 8.7$
7	1 g/L $\text{FeOOH}$ , 0 mM $\text{SiO}_2$	$0.562 \pm 0.005$	$1.23 \pm 0.01$
8	1 g/L $\text{FeOOH}$ , 0.5 mM $\text{SiO}_2$	$0.165 \pm 0.015$	$4.22 \pm 0.37$
9	1 g/L $\text{FeOOH}$ , 100 mM $\text{H}_2\text{O}_2$	$0.539 \pm 0.014$	$1.29 \pm 0.03$
10	1 g/L $\text{FeOOH}$ , 100 mM $\text{H}_2\text{O}_2$ , 0.5 mM $\text{SiO}_2$	$0.15 \pm 0.02$	$4.81 \pm 0.69$
11	5 g/L iron coated sand, 0 mM $\text{SiO}_2$	$0.134 \pm 0.012$	$5.21 \pm 0.45$
12	5 g/L iron coated sand, 0.5 mM $\text{SiO}_2$	$0.036 \pm 0.010$	$20.3 \pm 6.5$
13	4 g/L montmorillonite, 0 mM $\text{SiO}_2$ , $[\text{H}_2\text{O}_2]_{\text{initial}} = 50$ mM.	$0.0094 \pm 0.0008$	$74.4 \pm 6.6$
14	4 g/L montmorillonite, 0.5 mM $\text{SiO}_2$ , $[\text{H}_2\text{O}_2]_{\text{initial}} = 50$ mM.	$0.00283 \pm 0.00005$	$244.7 \pm 4.9$

Unless otherwise noted,  $[\text{H}_2\text{O}_2]_{\text{initial}} = 5$  mM,  $\text{pH} = 7$ ,  $[\text{NaNO}_3] = 0.1$  M. The rate constants were obtained by fitting the experimental data to the first order decay reaction rate law. The  $r^2$  values of the fittings were always  $r^2 > 0.99$ .

**Table 2**Possible surface complexation reactions between iron oxides and dissolved  $\text{SiO}_2$ 

	Reaction	Reference
$\equiv\text{FeOH} + \text{Si}(\text{OH})_4 \rightarrow \equiv\text{FeSiO}(\text{OH})_3 + \text{H}_2\text{O}$	(1)	11, 12, 30
$\equiv\text{FeOH} + \text{Si}(\text{OH})_4 \rightarrow \equiv\text{FeSiO}_2(\text{OH})_2^- + \text{H}_2\text{O} + \text{H}^+$	(2)	11, 12, 30
$\equiv\text{FeOH} + \text{Si}_2\text{O}_2(\text{OH})_5^- + \text{H}^+ \rightarrow \equiv\text{FeSi}_2\text{O}_2(\text{OH})_5 + \text{H}_2\text{O}$	(3)	12
$\equiv\text{FeOH} + \text{Si}_2\text{O}_2(\text{OH})_5^- \rightarrow \equiv\text{FeSi}_2\text{O}_3(\text{OH})_4^- + \text{H}_2\text{O}$	(4)	12
$2 \equiv\text{FeOH} + \text{Si}(\text{OH})_4 \rightarrow \equiv\text{Fe}_2\text{O}_2\text{Si}(\text{OH})_2 + 2 \text{H}_2\text{O}$	(5)	18, 28
$2 \equiv\text{FeOH} + 3 \text{Si}(\text{OH})_4 \rightarrow \equiv\text{Fe}_2\text{H}_{6-n}\text{Si}_3\text{O}_{10}^{n-} + n \text{H}^+ + 4 \text{H}_2\text{O}$	(6)	29